

Strongly-fluctuating moments in the high-temperature magnetic superconductor RbEuFe₄As₄

K. Willa,¹ R. Willa,¹ J.-K. Bao,¹ A. E. Koshelev,¹ D. Y. Chung,¹ M. G. Kanatzidis,^{1,2} W.-K. Kwok,¹ and U. Welp¹

¹*Materials Science Division, Argonne National Laboratory,
9700 South Cass Avenue, Lemont, IL 60439, USA*

²*Department of Chemistry, Northwestern University, Evanston, Illinois, 60208, USA*

(Dated: May 25, 2022)

The iron-based superconductor RbEuFe₄As₄ undergoes a magnetic phase transition deep in the superconducting state. We investigate the calorimetric response of RbEuFe₄As₄ single crystals of the magnetic and the superconducting phase and its anisotropy to in-plane and out-of-plane magnetic fields. Whereas the unusual cusp-like anomaly associated with the magnetic transition is suppressed to lower temperatures for fields along the crystallographic *c* axis, it rapidly transforms to a broad shoulder shifting to higher temperatures for in-plane fields. We identify the cusp in the specific heat data as a Berezinskii-Kosterlitz-Thouless (BKT) transition with fine features caused by the three-dimensional effects. The high-temperature shoulder in high magnetic fields marks a crossover from a paramagnetically disordered to an ordered state. This observation is further supported by Monte-Carlo simulations of an easy-plane 2D Heisenberg model and a fourth-order high-temperature expansion; both of which agree qualitatively and quantitatively with the experimental findings.

While superconductivity and magnetic order usually are mutually exclusive due to their competitive nature, a series of novel materials that feature the coexistence of both phases has recently emerged^{1–3}. In order to address open questions on the coexistence/interplay/competition between these two phases of matter, it is crucial to study model systems, where both phenomena can be tuned independently from each other. The Eu-based pnictide superconductors—where superconductivity occurs within the Fe₂As₂ layers, while the magnetism is hosted by the Eu²⁺ ions—provides such a model system³. Furthermore, each phenomenon appears to be relatively robust against perturbing the other one. In fact, chemical substitution of the parent non-superconducting compound EuFe₂As₂, e.g. with P (on the As site), K or Na (on the Eu site) induces superconductivity^{4–6} [with maximum T_c of 23K, 30K, and 35K respectively], while only smoothly suppressing the magnetic order temperature $T_m \sim 19$ K. Recent syntheses^{7,8} of members of the 1144 family (CsEuFe₄As₄ and RbEuFe₄As₄ with T_c in the mid-30K range) have opened new possibilities to tune the separation, and hence the interaction between neighboring Eu layers.

In this paper we report a detailed calorimetric characterization of single crystal RbEuFe₄As₄: in particular, we investigate the anisotropic response near the magnetic phase transition at $T_m = 14.9$ K (well within the superconducting state, $T_c = 37$ K) to external fields. Whereas earlier studies on polycrystalline samples⁸ have suggested that the magnetic transition might be of third (higher-than-second) order, we demonstrate that the behavior of the specific heat is broadly consistent with a Berezinskii-Kosterlitz-Thouless (BKT)^{9–11} transition with the Europium moments confined to the plane normal to the crystallographic *c* axis by crystal anisotropy. This finding is based on two main observations: first, the variation of the specific heat C in the vicinity of the phase transition agrees qualitatively and quantitatively with that of

a BKT transition. In particular, the BKT scenario naturally explains the absence of a singularity at the transition point. Furthermore, the anisotropic response of the specific heat to different field directions clearly points towards a strong ordering of the moments within the Eu planes. The reported findings are supported by numerical Monte-Carlo simulations of a classical anisotropic 2D Heisenberg spin system.

Generally speaking, a BKT transition means that the state above the critical temperature can be viewed as a liquid of magnetic vortices and antivortices, while in the low temperature ordered phase only bound vortex-antivortex pairs are present. In a pure 2D case the average magnetic moment would thus be destroyed by spin-wave fluctuations also in the ordered phase. Weak interlayer coupling, as present in RbEuFe₄As₄, promotes a small average in-plane moment formed at very large scales, while at smaller scale the behavior remains two-dimensional. This results in the fact, that the true phase transition in this system belongs to the universality class of the three-dimensional anisotropic Heisenberg model. However, these 3D effects are only relevant within a narrow range near the transition temperature and add fine features on the top of overall 2D behavior. Similar scenarios are realized in several layered magnetic compounds, such as K₂CuF₄^{12,13} and Rb₂CrCl₄^{14,15}.

The appearance of the superconducting phase below $T_c = 36.8(6)$ K and a magnetic phase below $T_m = 14.9$ K are clearly revealed in the calorimetric data obtained on zero-field cooling from room temperature down to 2K, see Fig. 1. Whereas the superconducting transition temperature is extracted through an entropy conserving construction, see Fig. 1(f), we determine the magnetic transition temperature from the position of the specific-heat cusp, which does not show signs of a first- or second-order phase transition. This observation is in line with previously reported results on polycrystalline CsEuFe₄As₄⁷ and RbEuFe₄As₄⁸, and should be contrasted to results on

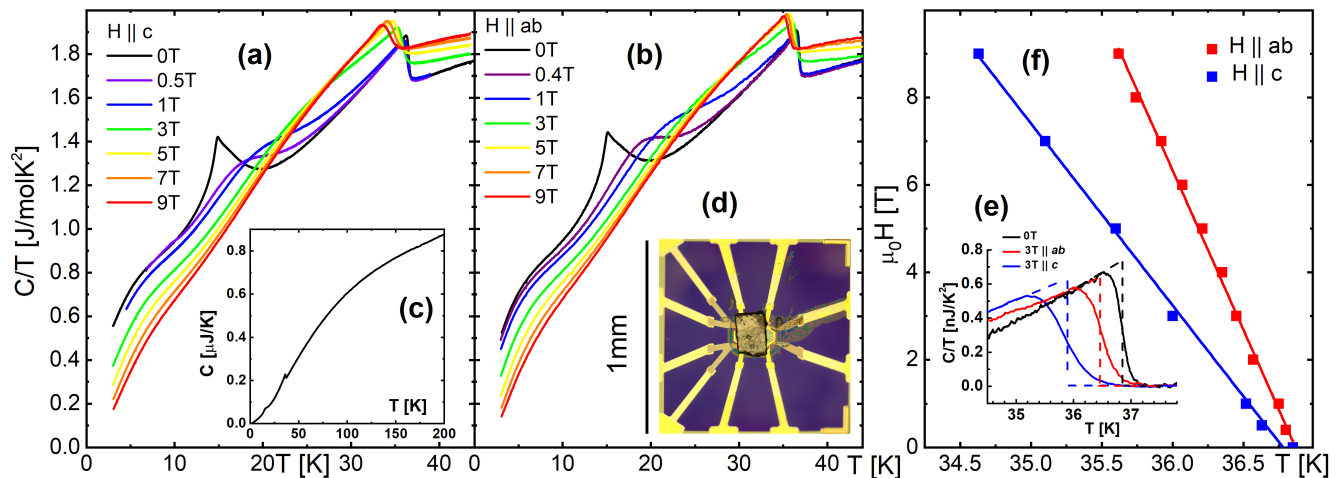


FIG. 1. Entropy change (C/T) in single crystal $\text{RbEuFe}_4\text{As}_4$ and its dependence on the magnetic field strength when applied along (a) and perpendicular (b) to the crystallographic c axis. The superconducting transition at $T_c = 37\text{K}$ and the magnetic transition at 15K are clearly visible in the zero-field calorimetric scan (c), as obtained from a room-temperature cool down. The microscope image (d) shows the ac nanocalorimeter platform with a $\text{RbEuFe}_4\text{As}_4$ single crystal mounted at its center. Following the evolution of the superconducting transition in an applied field, (e), allows to extract the phase diagram (f) and to evaluate the superconducting anisotropy $\Gamma = 1.8$. The apparent discrepancy in the extrapolated T_c is within the experimental uncertainty.

EuFe_2As_2 which show a singularity^{16–19}. The variation of the specific heat in the vicinity of the phase transition, the specific heat can be expressed²⁰ as $C = a^\pm |t|^{-\alpha} + b(t)$. The first term captures the critical behavior near $t = 0$ with $t = T/T_m - 1$ the reduced temperature, a^\pm the critical amplitudes for $t < 0$ (–) and $t > 0$ (+), and α the critical exponent. The second term captures all regular contributions (e.g. from phonons) and is typically modeled by a linear form $b(t) = b_0 + b_1 t$ in a small temperature range around the transition. A non-divergent specific heat implies $\alpha < 0$, and hence the constant $b_0 \equiv C(T_m)$ assumes the value of the specific heat at the transition temperature. For each branch $t \leq 0$, we find a critical exponent $\alpha \approx -1$; a highly unusual value. For the critical amplitudes we find $a^+ = 18.5\text{J/molK}$ and $a^- = 4.76\text{J/molK}$ respectively, see fits in Fig. 2.

Contrary to earlier speculations⁸, we find that this transition with non-singular behavior is consistent with a Berezinskii-Kosterlitz-Thouless transition of the Eu^{2+} magnetic moments weakly influenced by 3D effects. A uniaxial anisotropy forces the moments to orient within the crystallographic ab plane, effectively reducing the moment's degrees of freedom to that of a 2D XY spin system. A more detailed justification shall be given below. The down-bending of the calorimetric data below $\sim 10\text{K}$ is attributed to the quantum nature of the high spin Eu^{2+} moments^{21–23}. In applied fields, the superconducting transition temperature is gradually suppressed; the effect is stronger, if the field is applied along the c axis. The rate of T_c -suppression $dT_c/dH|_{ab} = 0.14\text{K/T}$ and $dT_c/dH|_c = 0.25\text{K/T}$, provides a uniaxial *superconducting* anisotropy of $\Gamma = 1.8$, as shown in Fig. 1. These values agree with complementary magnetization and transport

measurements^{23,24} on single crystal $\text{RbEuFe}_4\text{As}_4$. No influence on the step height $\Delta C/T$ or the phase boundary from magnetism is detected in fields up to 9T. In high fields, $0.4\text{T} < \mu_0 H < 9\text{T}$, the cusp of the magnetic transition evolves into a broad magnetic hump with its center moving to higher temperatures. At the highest field (9T) these magnetic fluctuations extend up to about 100K—far above the superconducting transition—and provide a natural explanation for the reported negative, normal-state magneto-resistance²³. We attribute this hump to a field-induced polarization of the Eu^{2+} moments along the field direction and their associated fluctuations.

For a more detailed analysis of the magnetic transition, we performed low-field calorimetric scans in the vicinity of T_m . Given the robust superconductivity (low dT_c/dH) and the clear separation of energy scales $k_B T_m \ll k_B T_c$, the (low-)field changes in the calorimetric data can be attributed to the magnetism. To accentuate these, we have to subtract an overall background. However, subtracting a phonon-type background turns out difficult because of other (in particular superconducting) contributions. We therefore subtract the 9T specific heat data (field along c axis). While the latter still contains magnetic and superconducting contributions, both are essentially featureless in the temperature range of interest, see Fig. 1. As shown in Fig. 2, for small applied fields along the c axis, the specific-heat cusp at the magnetic transition shifts to lower temperatures while broadening slightly and a shoulder in the specific heat appears on the high-temperature side. Defining the phase boundary $T_m(H)$ as the position of the cusp, see Fig. 3, a mean-field fit provides the empiric law $T_m(H) = T_m[1 - (H/H_0)^2]$, with $\mu_0 H_0 \approx 0.93\text{T}$. This suggests that at this field value

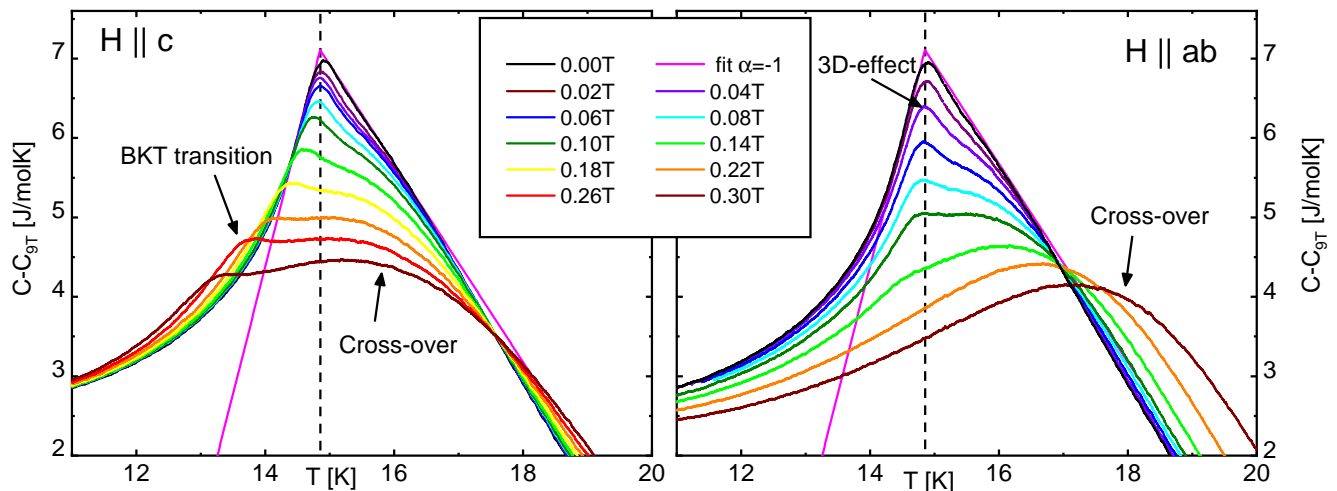


FIG. 2. specific heat subtracted by the 9T background curve around the magnetic transition upon applying fields from 0.02 to 0.3T out-of-plane (left) and in-plane (right). The sharp kink indicating the ordering of the Eu^{2+} moments in the plane while the broad hump developing at higher temperatures shows the gradual magnetization of the sample parallel to the applied field.

the planar anisotropy is overcome at all temperatures, i.e. at zero temperature the magnetic moments fully align with the field normal to the ab plane. A comparable saturation field can be deduced from low-temperature magnetization curves²³. For in-plane fields, the position of the cusp is almost field-independent, while its size is readily suppressed (disappearing at 0.14T) and a pronounced shoulder appears on the high-temperature side. As discussed below, we attribute the cusp to a weak 3D coupling between Eu layers. The appearance of the high-temperature feature marks the onset of magnetic polarization, as discussed above. This hump is not a sharp phase boundary but should rather be understood as a crossover from a paramagnetically disordered to an ordered state. Due to anisotropy effects, this occurs more rapidly for in-plane than for out-of-plane fields.

Further insight into the response of $\text{RbEuFe}_4\text{As}_4$ is gained through a detailed study of a model spin system describing the key features of this compound, implemented using a Monte-Carlo^{25,26} algorithm, see Supplementary Material B. More specifically, we have investigated the magnetic and thermodynamic properties of a two-dimensional square lattice of [Heisenberg-type, $\mathcal{O}(3)$] classical spins \mathbf{s}_i governed by the Hamiltonian

$$\mathcal{H} = -J \sum_{\langle i,j \rangle} \mathbf{s}_i \cdot \mathbf{s}_j + K \sum_i (2s_{i,z}^2 - 1) - \mathbf{h} \cdot \sum_i \mathbf{s}_i. \quad (1)$$

Here J defines the isotropic coupling between nearest-neighbor spin pairs $\langle i,j \rangle$, K introduces a uniaxial anisotropy in spin space. The last term describes the coupling to an external magnetic field \mathbf{h} . Without limiting the generality of the foregoing, we set $|\mathbf{s}_i| = 1$. A similar approach has been extensively used in the past to explore the 2D XY model, see Refs. [27–31].

The simulated system is purely two-dimensional, and hence neglects the coupling between neighboring Eu lay-

ers. This choice is motivated by the observation that the parent non-superconducting compound EuFe_2As_2 displays small interlayer interactions compared to the intralayer interactions. We expect the coupling between Eu layers to be even weaker in $\text{RbEuFe}_4\text{As}_4$, as the separation between Eu layers doubled and two superconducting layers are in between. The interlayer coupling becomes relevant only at temperatures near the transition and for small magnetic fields. In the Hamiltonian (1), the spin anisotropy is modeled by a crystalline term $\propto s_{i,z}^2$. The

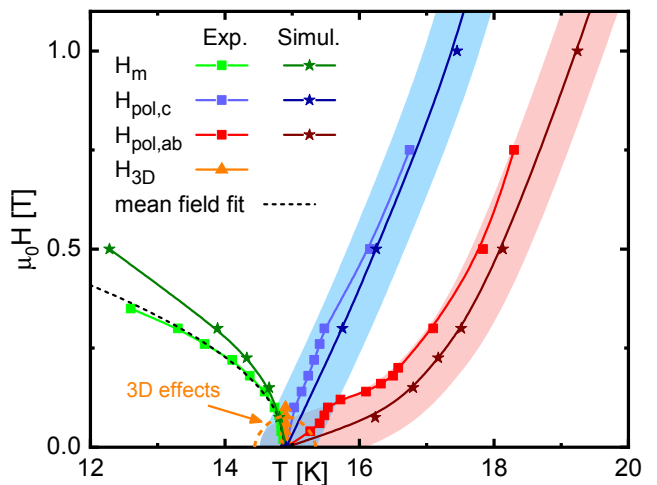


FIG. 3. Boundaries of the magnetic phase as obtained from measured and simulated calorimetric data. The transition to an ordered magnetic phase is shown by green symbols, and agrees well with the empiric law $H_m = H_0(1-T/T_m)^{1/2}$, when the field is applied along the c -axis. A broad hump in the specific heat marks the crossover to a field-driven polarized state of Eu^{2+} moments and is shown for fields parallel (blue) and normal (red) to the c axis.

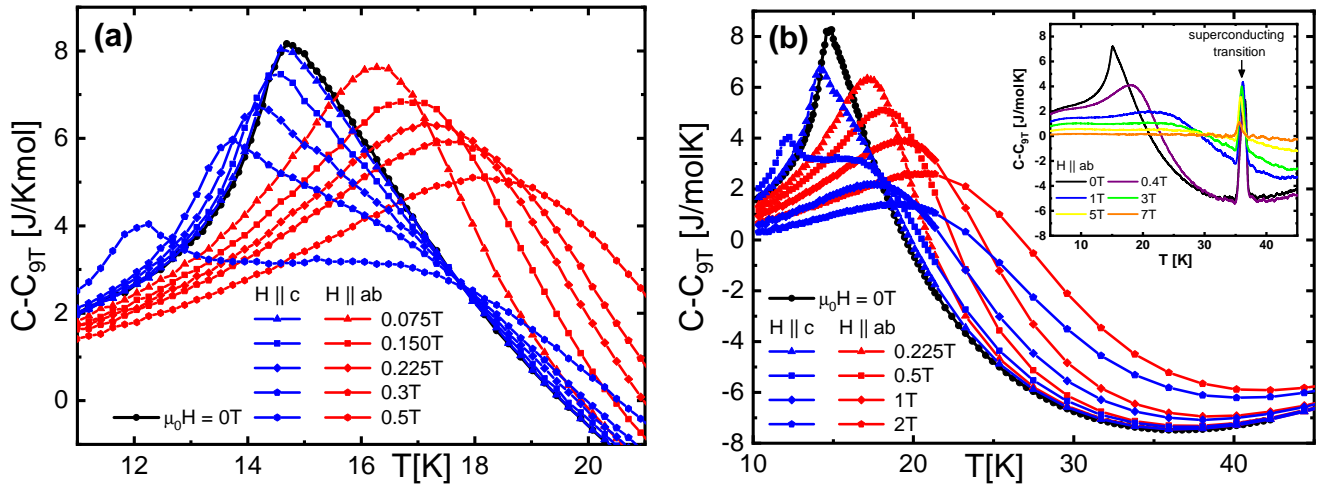


FIG. 4. Simulated specific heat of the anisotropic 2D Heisenberg spin system and its dependence on temperature for different magnetic fields and their orientations; red (in-plane), blue (out-of-plane), black (zero-field). For all curves the 9T-background data is subtracted [conversion to real units using Eq. (2)]. (a) shows the low-field features and their anisotropic response near the magnetic transition. The specific heat at larger fields, and over a wider temperature range, is shown in (b). The experimental signature of the superconducting transition near 37K, see inset, is not captured in the simulations.

Eu^{2+} ions have a vanishing angular momentum ($L = 0$), which excludes a crystalline anisotropy originating from spin-orbit coupling. However, the coupling between the Eu^{2+} moments and Fe d -electrons—the latter are known to feature an easy-plane anisotropy^{32,33}—naturally leads to such a term, see Supplementary Material D. Other sources of anisotropy such as dipolar interactions, considered elsewhere³⁴, are neglected. The anisotropic term causes the system to fall into the universality class of 2D XY spin systems, where a BKT transition is known to occur at a finite temperature $T_m > 0$ ³⁵. In contrast to our model, an isotropic (in spin space) 3D Heisenberg model with anisotropic nearest neighbor coupling (J in-plane vs. $J' = \lambda J$ between Eu layers) fails to capture an anisotropic susceptibility, while the isotropic (in spin space) two-dimensional Heisenberg model does not undergo a phase transition at finite temperatures^{36–39}.

We investigate several response functions in this system: the (direction-dependent) magnetic susceptibility $\chi_\alpha(T)$ ($\alpha = x, y, z$), the specific heat $C(T, \mathbf{h})$, the total magnetization $\mathbf{S}(T, \mathbf{h}) = \sum_i \mathbf{s}_i$, and the spin-spin correlation function $G(r) \equiv \langle \mathbf{s}(0)\mathbf{s}(r) \rangle$. For convenience we introduce the temperature scale $T_0 \equiv J/k_B$. From high-temperature simulations (typically $T/T_0 \in [4, 9]$), we fit the inverse magnetic susceptibility to a Curie-Weiss law $\chi_\alpha^{-1}(T) \propto T - \Theta_{C,\alpha}$ to extract the Curie temperatures $\Theta_{C,\alpha}$. A comparison between the measured and the simulated susceptibility can be found in the Supplementary Material C3. Any non-zero value of K results in an anisotropy between the in-plane ($\Theta_{C,x}$) and out-of-plane ($\Theta_{C,z}$) Curie temperature. By comparing the anisotropy ratio $\Theta_{C,x}/\Theta_{C,z}$ with the reported²³ value 1.075 for $\text{RbEuFe}_4\text{As}_4$ obtained from magnetization measurements, we find an agreement for the specific value $K = 0.1J$, where $\Theta_{C,x} = 1.20T_0$ and $\Theta_{C,z} = 1.12T_0$. All

further simulations are performed for this anisotropy parameter. The influence of the anisotropy parameter on the shape of $C(T)$ dependence at $h = 0$ and the location of the cusp is considered in the Supplementary Material C4.

In zero magnetic field, the simulated specific heat shows a clear cusp at $T_m/T_0 = 0.7$, a value that we identify with the transition temperature $T_m = 14.9\text{K}$ of the calorimetric experiment. It is known however, that the true BKT transition temperature T_{BKT} is slightly below the specific heat cusp. The correlation function is expected to decay as a power law $r^{-1/4}$ at the transition, providing a value $T_{\text{BKT}} = 0.66T_0$, i.e., about 6% below the cusp in the specific heat. At the same time, the correlation function decays as $G(r) \propto \exp[-r/\zeta(T)]$, with a correlation lengths $\ln[\zeta(T)] \propto (T - T_{\text{BKT}})^{-1/2}$ that diverges upon approaching the transition from above. Evaluation of $\zeta(T)$ and its singular behavior yields a consistent result, see Supplementary Material C2.

At finite fields, the calorimetric and magnetic responses strongly depend on the field orientation. For fields applied along the spin plane, the $U(1)$ circular degeneracy is lifted and no BKT transition occurs. The system's response follows a typical ferromagnetic behavior (gradual magnetization upon cooling) reaching a fully ordered state at lowest temperatures. The specific heat gradually broadens and shifts to higher temperatures. On the contrary, a field applied perpendicular to the spin lattice preserves the $U(1)$ rotational symmetry and the BKT transition shifts to lower temperatures. Here the magnetic field acts as an anisotropic term favoring the spin orientation along the z axis, hence retarding the transition to an in-plane spin orientation. The numerical simulations are in excellent qualitative and quantitative agreement with the experimental data, see Figs. 2

and 4. Additionally, the simulations reproduce the behavior of the magnetization and the susceptibility which is discussed in the Supplementary Material C3. The phase boundaries extracted from the simulation data (converted to appropriate units) are shown in Fig. 3. The green curve corresponds to the suppression of the BKT transition due to a field normal to the spin plane. The two other curves correspond to a crossover where magnetic moments are polarized along the field (blue, $H\|c$ and red, $H\|ab$). The simulation result reproduces the experimental data extremely well, with only minor deviations for low fields along the ab plane. This difference is attributed to 3D-effects close to the transition, that are not accounted for in the simulations.

Having identified realistic values for the dimensionless parameters T/T_0 (from calorimetry) and K/J (from high-temperature magnetization), we can rewrite the model Hamiltonian in Eq. (1) in a dimensional form

$$\mathcal{H}_{\text{real}} = -\mathcal{J} \sum_{\langle i,j \rangle} \mathbf{m}_i \mathbf{m}_j + 2\mathcal{K} \sum_i m_{i,z}^2 - \mathbf{H} \mathbf{M}, \quad (2)$$

where a constant shift has been omitted. Here $\mathbf{M} = \sum_i \mathbf{m}_i$ denotes the total magnetization of the individual constituents $|\mathbf{m}_i| \approx 7\mu_B$, $\mathcal{J} = 0.6 \times 10^{-23} \text{J}/\mu_B^2$ ($= 10\mathcal{K}$) providing the relevant energy scale for the ferromagnetic interactions (the anisotropy). It is useful to express the simulated fields h in dimensional units via $h \rightarrow \mu_0 H = 4.53h[\text{T}]$.

The numerical results are backed up by a high-temperature expansion of the model described by Eq. (1), see Supplementary Material C1. Here the anisotropy ratio in the Curie temperature takes the simple form

$$\Theta_{C,x}/\Theta_{C,z} = (1 + K/5J)/(1 - 2K/5J) \quad (3)$$

and yields the value 1.06 for $K = 0.1J$. This relation reiterates that for an easy-plane anisotropy $K > 0$ the ratio of Curie temperatures $\Theta_{C,x}/\Theta_{C,z}$ is larger than unity, whereas an easy-axis system ($K < 0$) has $\Theta_{C,x}/\Theta_{C,z} < 1$. Note that the sign of the anisotropy may change for different Eu-containing compounds. We find that the presumed 'high-temperature' range $T/T_0 \in [4, 9]$ (corresponding to 50–200K) is only captured properly when the high-temperature expansion is taken to quartic order in $\beta\mathcal{H}$ [the susceptibility is expanded to cubic order in $\beta = (k_B T)^{-1}$]. This explains the noticeable discrepancy between the 'exact' values $\Theta_{C,x}/T_0 = 4/3 + 4K/15J$ ($= 1.36$) and $\Theta_{C,z}/T_0 = 4/3 - 8K/15J$ ($= 1.28$) obtained in the high-temperature limit and their numerical counterparts 1.20 and 1.12, see above.

We have assumed that the third dimension, perpendicular to the easy-plane, plays a marginal role in the calorimetric response of the magnetic order. A weak coupling $J' = \lambda J$ ($|\lambda| \ll 1$) between ferromagnetically ordered Eu layers will add a fine structure on top of the leading features. Very close to the transition, when the correlation length $\zeta(T)$ reaches the in-plane length scale $1/\sqrt{\lambda}$ at the temperature³⁵ $T - T_m \sim T_m \ln^{-2}(1/\lambda)$, the three-dimensional effects lead to full ordering of the system.

On general ground, these effects should sharpen the specific heat cusp in close vicinity of the transition^{28,31}. The nature of this three-dimensional order depends on the interlayer interactions: while a simple coupling J' between neighboring layers results in a trivial ferro- ($J' > 0$) or A-type antiferromagnet ($J' < 0$), more complicated helical, and fan-like orders can be found if longer-range interactions along z are considered^{40,41}. In the latter cases there is the typical in-plane magnetic field scale $B_{3D} = J'/|\mathbf{m}|$ aligning the moments in different layers in the same directions and eliminating the magnetic transition.

In conclusion, we have investigated the magnetic transition in $\text{RbEuFe}_4\text{As}_4$ by specific heat measurements and by Monte-Carlo simulations. The magnetic transition at 14.9K shifts to lower temperatures in fields along the c axis. This is well reproduced by the simulations of the 2D anisotropic Heisenberg system. This allows us to identify the ab plane as the magnetic easy plane and the specific-heat curve indeed shows a dominant BKT character. A magnetic field normal to the Eu layers shifts the magnetic transition to lower temperature. Applying the field along the Eu planes lifts the rotational symmetry required for a BKT transition. The latter is replaced by a broad crossover from a paramagnetically disordered to an field-ordered state. With a quantitative comparison between our simulation and experimental data, we have extracted the coupling constants $\mathcal{J} = 0.6 \times 10^{-23} \text{J}/\mu_B^2$ and the anisotropy $\mathcal{K} = 0.1\mathcal{J}$. The extraction of the phase boundary of the BKT transition and the crossover lines for in- and out-of-plane fields further underline the excellent agreement between experiment and simulations.

The unique feature of $\text{RbEuFe}_4\text{As}_4$ is that the magnetic transition takes place deep inside the superconducting phase. We expect that the superconductivity has almost no influence on the intralayer exchange interaction between Eu moments and may only modify the interlayer interactions. Therefore, the direct impact of superconductivity on magnetism is likely to be minor. The effects caused by the opposite influence of magnetism on superconductivity are expected to be more pronounced. The presence of the magnetic subsystem with a large susceptibility drastically modifies the macroscopic magnetic response of the superconducting material in the mixed state⁴². The source of the microscopic interaction between the magnetic and superconducting subsystems is an exchange coupling between the Eu moments and Cooper pairs. Even though this coupling is not strong enough to completely destroy superconductivity, like, e.g., in ErRh_4B_4 ⁴³, it may cause a noticeable suppression of superconducting parameters at the magnetic transition. Having established the nature of the robust magnetic order, this work serves as a starting point for further exploring the phenomena related to the influence of magnetism on the superconducting state.

ACKNOWLEDGMENTS

We are thankful for the helpful discussions with Matthew Smylie and Andreas Rydh. This work was supported by the U.S. Department of Energy, Office of Science, Basic Energy Sciences, Materials Sciences and Engineering Division. K. W. and R.W. acknowledge support from the Swiss National Science Foundation through an Early Postdoc Mobility fellowship.

Supplementary Material

A: Experiment

For our calorimetry experiment, we mounted a small, platelet-shaped RbEuFe₄As₄ single crystal, grown in RbAs flux⁴⁴, onto a nanocalorimeter platform^{45,46} using Apiezon grease, see Fig. 1. The probe was then inserted into a three axis vector magnet (1T-1T-9T), where the field axes were aligned with the crystal axes within ± 3 degrees. The specific heat data, as obtained from *ac* measurements ($f = 1\text{Hz}$ and $\delta T \sim 0.1\text{K}$), was recorded with a Synktext lock-in amplifier.

B: Numerical routine

Given a spin configuration, a Monte-Carlo iteration step consists in evaluating the energy change δE induced by virtually substituting an existing spin \mathbf{s}_i at site i by a new spin $\tilde{\mathbf{s}}_i$. If δE is negative, the replacement $\mathbf{s}_i \rightarrow \tilde{\mathbf{s}}_i$ is effected. In the opposite case $\delta E > 0$, the replacement is performed with a reduced probability $p = \exp(-\delta E/T)$. Numerically, this evaluation and update procedure is particularly suited for local Hamiltonians, where each spin only interacts with few neighboring spins. Repeating this step for each spin of the lattice then defines one *pass*. Thermal properties such as the system's average energy, magnetization, and their respective fluctuations can then be studied by evolving the system through many passes. In general, the new spin $\tilde{\mathbf{s}}_i$ is chosen by picking a random unit vector. At low temperatures, however, when the rate of accepted spin changes drops below a certain threshold (typically 0.5), we reduce the explored phase space to a cone centered around \mathbf{s}_i and with an opening angle Ω , i.e. $\arccos(\mathbf{s}_i \tilde{\mathbf{s}}_i) \leq \Omega$. The value of $\Omega \leq \pi$ is adjusted to yield an acceptance rate close to the threshold acceptance rate.

In our implementation, we simulate a square lattice of $L \times L$ spins (typically $L = 100$); initialized in a random spin configuration (the same for each run). Given a fixed parameter set (T, \mathbf{h}) (all simulations shown in the main text are obtained with $J = 10K = 1$), we run the simulation through $N_p/2$ passes for thermalization after which observable quantities and their fluctuations are evaluated over the next N_p passes. The spins are visited typically $N_p = 10^7$ times in a random order (reshuffled after each pass). The total energy E , its square, the total magnetization $\mathbf{S} = \sum_i \mathbf{s}_i$, and its component's square are (time-)averaged over 10^4 - 10^5 passes and written to file for post-processing.

The magnetic susceptibility and the specific heat (both per spin) are derived from the above quantities via

$$\chi_\alpha = \frac{1}{L^2} \frac{\langle S_\alpha^2 \rangle - \langle S_\alpha \rangle^2}{k_B T} \quad \text{and} \quad C = \frac{k_B}{L^2} \frac{\langle E^2 \rangle - \langle E \rangle^2}{(k_B T)^2} \quad (\text{B1})$$

respectively. An equivalent expression for the specific heat be $L^{-2} \partial \langle E \rangle / \partial T$ was used to check the accuracy of the results.

C: Properties the anisotropic 2D Heisenberg model

1. High-temperature expansion

When writing the Hamiltonian (1) using the spin representation $\mathbf{s}_i = (\cos \phi_i \sin \theta_i, \sin \phi_i \sin \theta_i, \cos \theta_i)$ we find

$$\mathcal{H} = -J \sum_{\langle i,j \rangle} [\sin \theta_i \sin \theta_j \cos(\phi_i - \phi_j) + \cos \theta_i \cos \theta_j] + K \sum_i \cos(2\theta_i) - \sum_i [h_x \cos \phi_i \sin \theta_i + h_y \sin \phi_i \sin \theta_i + h_z \cos \theta_i]. \quad (\text{C1})$$

The system's partition function reads $Z = \langle\langle \exp(-\beta \mathcal{H}) \rangle\rangle$ with $\beta = (k_B T)^{-1}$ and $\langle\langle \dots \rangle\rangle = \prod_i (4\pi)^{-1} \int \dots \sin \theta_i d\theta_i d\phi_i$ the uniform average over the unit sphere. Observable quantities can be evaluated from the free energy per spin $F = \ln(Z)/\beta N$, which (at high temperatures) can be approximated by

$$F \approx F^{(4)} \equiv \frac{-1}{\beta N} \left[-\beta \langle\langle \mathcal{H} \rangle\rangle + (\beta^2/2)(\langle\langle \mathcal{H}^2 \rangle\rangle - \langle\langle \mathcal{H} \rangle\rangle^2) - (\beta^3/6)(\langle\langle \mathcal{H}^3 \rangle\rangle - 3\langle\langle \mathcal{H}^2 \rangle\rangle \langle\langle \mathcal{H} \rangle\rangle + 2\langle\langle \mathcal{H} \rangle\rangle^3) \right. \\ \left. + (\beta^4/24)(\langle\langle \mathcal{H}^4 \rangle\rangle - 4\langle\langle \mathcal{H}^3 \rangle\rangle \langle\langle \mathcal{H} \rangle\rangle - 3\langle\langle \mathcal{H}^2 \rangle\rangle^2 + 12\langle\langle \mathcal{H} \rangle\rangle^2 \langle\langle \mathcal{H}^2 \rangle\rangle - 6\langle\langle \mathcal{H} \rangle\rangle^4) \right] \quad (\text{C2})$$

to fourth order in \mathcal{H} , where $\langle\langle \mathcal{H}^n \rangle\rangle$ is the n -th moment of the Hamiltonian. Going through the calculation of each moment, one finally arrives at the expression

$$F^{(4)} = -K/3 - \beta \left[\frac{J^2}{3} + \frac{8K^2}{45} + \frac{h^2}{6} \right] - \beta^2 \left[\frac{2Jh^2}{9} - \frac{64K^3}{2835} + \frac{2K(h_x^2 + h_y^2 - 2h_z^2)}{45} \right] \\ - \beta^3 \left[\frac{7J^4}{270} - \frac{64K^4}{14175} - \frac{h^4}{180} + \frac{32J^2K^2}{675} + \frac{2J^2h^2}{9} + \frac{112JK - 8K^2}{945} (h_x^2 + h_y^2 - 2h_z^2) \right] \quad (C3)$$

Whereas up to linear order in β the anisotropic term $\propto K$ merely shifts the energy, the spin response becomes truly anisotropic with the term $\propto \beta^2 K h_\alpha^2$. The specific heat per spin $C = -k_B \beta^2 dU/d\beta$ is obtained from the average energy per spin $U = -(1/N)d \ln Z/d\beta = d(\beta F)/d\beta$ and amounts to

$$C = k_B \beta^2 \left\{ \left(\frac{2J^2}{3} + \frac{16K^2}{45} \right) - \beta \frac{128K^3}{945} + \beta^2 \left(\frac{14J^4}{45} + \frac{128J^2K^2}{225} - \frac{256K^4}{4725} \right) \right. \\ \left. + \frac{h^2}{3} + \beta \left[\frac{4Jh^2}{3} + \frac{4K}{15} (h_x^2 + h_y^2 - 2h_z^2) \right] + \beta^2 \left[\frac{8J^2h^2}{3} + \frac{32(14J - K)K}{315} (h_x^2 + h_y^2 - 2h_z^2) - \frac{h^4}{15} \right] \right\}. \quad (C4)$$

Here the first line corresponds to the zero-field limit and the second line includes all field terms. Components of the average spin are obtained from $s_\alpha = (1/\beta N)d \ln Z/dh_\alpha = -dF/dh_\alpha$, and the susceptibilities $\chi_\alpha = \lim_{h \rightarrow 0} [s_\alpha/h_\alpha]$ read

$$\chi_x = \chi_y = \frac{\beta}{3} + \beta^2 \left(\frac{4J}{9} + \frac{4K}{45} \right) + \beta^3 \left(\frac{4J^2}{9} + \frac{32JK}{135} - \frac{16K^2}{945} \right) \quad (C5)$$

$$\chi_z = \frac{\beta}{3} + \beta^2 \left(\frac{4J}{9} - \frac{8K}{45} \right) + \beta^3 \left(\frac{4J^2}{9} - \frac{64JK}{135} + \frac{32K^2}{945} \right) \quad (C6)$$

For high temperatures $J\beta \ll 1$, the susceptibility follows a Curie-Weiss law $\chi_\alpha \approx \chi_0^\alpha / (T/\Theta_{C,\alpha} - 1)$, with $\Theta_{C,\alpha}$ the orientation-dependent Curie-Weiss temperature, and χ_0^α a constant. We have

$$\chi_0^x = \chi_0^y = 5/[4(5J + K)] \quad \chi_0^z = 5/[4(5J - 2K)] \quad (C7)$$

$$k_B \Theta_{C,x} = k_B \Theta_{C,y} = (4/15)(5J + K) \quad k_B \Theta_{C,z} = (4/15)(5J - 2K) \quad (C8)$$

When measuring the inverse susceptibility, the curves along x and z are shifted by a constant, whereas the slopes $1/\chi_0^\alpha \Theta_{C,\alpha}$ are the same. The ratio of the two Curie temperatures (in-plane vs. out-of-plane) then reads $\Theta_{C,x}/\Theta_{C,z} = (5 + K/J)/(5 - 2K/J)$, while the sign of the Curie-Weiss temperature indicates whether the spin coupling is dominantly ferromagnetic ($J > 0$) or antiferromagnetic ($J < 0$), the ratio $\Theta_{C,x}/\Theta_{C,z}$ is informative about the nature of the anisotropy. In fact the system is an easy-plane (XY -type) magnet if $\Theta_{C,x}/\Theta_{C,z} > 1$. If $\Theta_{C,x}/\Theta_{C,z} < 1$ the magnet has easy axis (Ising-type) with moments orienting preferentially normal to the spin plane.

2. Behavior of the correlation functions and the exact location of the BKT temperature

As mentioned in the main text, the cusp in specific heat just corresponds to an approximate location of the transition. In contrast to conventional magnetic transitions, the long-range order does not emerge below T_{BKT} . In order to extract the true BKT transition temperature, we have to analyze the moment correlation function $G(\mathbf{r}) = \langle s(0)s(\mathbf{r}) \rangle$. The long-range behavior of $G(\mathbf{r})$ changes qualitatively at T_{BKT} , it decays exponentially in the paramagnetic state $G(\mathbf{r}) \propto \exp(-r/\zeta)$ and below T_{BKT} the decay is algebraic $G(\mathbf{r}) \propto r^{-\beta}$. Moreover, as follows from the theory of the BKT transition¹¹, the moment correlation length diverges as $\zeta(T) \propto \exp[b\sqrt{T_{\text{BKT}}/(T - T_{\text{BKT}})}]$ for $T \rightarrow T_{\text{BKT}} + 0$ and the value of the power exponent β at T_{BKT} is exactly $1/4$. Figure 5 shows temperature dependence of the power exponent β and the correlation length ζ extracted from fits of the numerically computed correlation function. Extracting the true transition temperatures below ($T_{\text{BKT}}^< = 0.66T_0$) and above ($T_{\text{BKT}}^> \approx 0.67T_0$) leads us to conclude, that the transition is at $T_{\text{BKT}} = 0.67T_0$ which is 5% below the cusp position seen at $T_m = 0.7T_0$.

3. Behavior of susceptibility and magnetization

We have investigated to some detail the magnetic response of the spin system for the anisotropy $K = 0.1J$ (discussed in the main text). Figure 6 compares the temperature dependencies of the computed linear susceptibilities and the

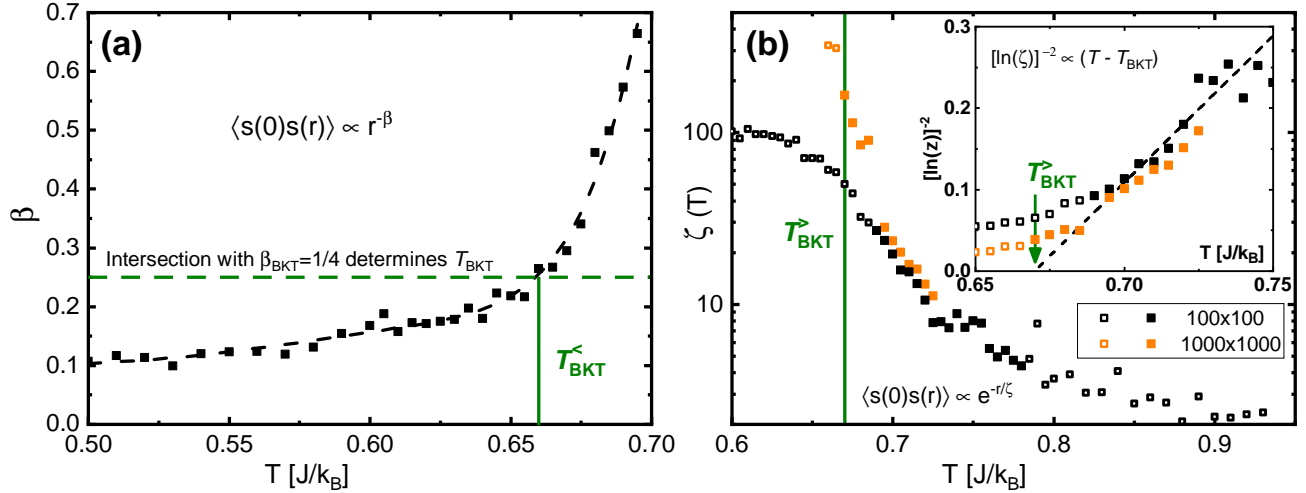


FIG. 5. An accurate definition of the BKT transition temperature involves studying the temperature-dependence of the correlation function $G(r) = \langle \mathbf{s}(0)\mathbf{s}(r) \rangle$. **(a)** Below T_{BKT} , the latter decays as a power law $G(r) \propto r^{-\beta}$ with $\beta_{\text{BKT}} = 1/4$. The intersection of a fit (black dashed) with $1/4$ provides $k_B T_{\text{BKT}}^< / J = 0.66$. **(b)** Above the transition, the correlation length decays exponentially, $G(r) \propto e^{-r/\zeta}$, with the correlation length $\ln \zeta(T) \propto (T - T_{\text{BKT}})^{-1/2}$. The linear fit $[\ln(\zeta)]^{-2} = -2.41 + 3.60T/T_0$ (black dashed) to the black and orange filled symbols provides $T_{\text{BKT}}^> \approx 0.67T_0$. This extraction is more sensitive to the system's finite size, as it requires to approach very close to the transition, where the correlation length diverges. Shown here is the correlation length for the typical system (100×100 spins, black) and selected points have been computed for a large system (1000×1000 spins, orange).

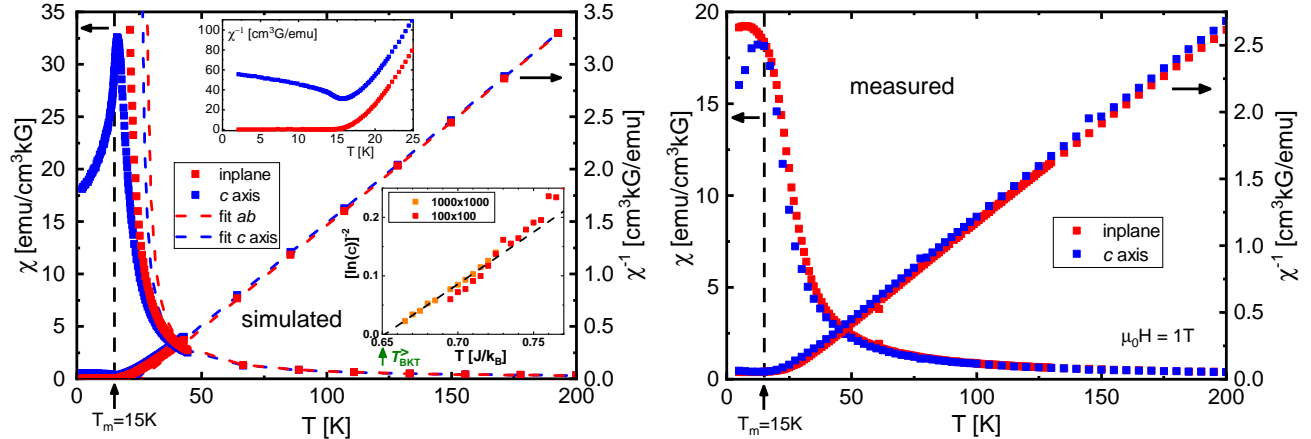


FIG. 6. Comparison of the simulated linear susceptibilities (*left*) and the measured susceptibilities at fixed magnetic field $\mu_0 H = 1\text{T}$ (*right*, published earlier in Ref. [23]). The simulated susceptibility has been converted to real units by using the density of 0.5×10^{22} Europium atoms per cm^3 . The dashed lines in the simulation plot show fits to the Curie-Weiss dependence discussed in the main text and the higher inset highlights the susceptibility's low-temperature dependence. The lower inset verifies the BKT scaling $[\ln(\chi(T))]^{-2} = -1.16 + 1.78T/T_0$ expected near the transition giving a transition at $T_{\text{BKT}}^> \approx 0.65T_0$ close to the value extracted from the correlation length.

measured susceptibilities at fixed magnetic field²³ $\mu_0 H = 1\text{T}$. The comparison is only justified above 30 K, because, as evident from Fig. 7, the susceptibility at lower temperatures becomes nonlinear at this field. Furthermore, the behavior of the experimental susceptibility data at smaller fields is strongly influenced by the appearance of superconductivity. In the high-temperature range the model describes well the temperature dependencies of susceptibilities and their anisotropy. A linear fit to the high-temperature part of the measured inverse susceptibility leads to the Curie temperatures for the in- and out-of-plane directions. This information was extracted and used to determine the anisotropy parameter for the simulations.

In the vicinity of the BKT transition, the linear susceptibility diverges as $\chi(T) \propto \zeta^2 \propto \exp[2b\sqrt{T_{\text{BKT}}/(T - T_{\text{BKT}})}]$. The simulated susceptibility indeed shows this behavior, as illustrated in the lower inset of Fig. 6 (left), where we plot

the temperature dependence of $[\ln(\chi)]^{-2}$ for two system sizes. The linearity of this dependence indicates the validity of the BKT scaling. The slope should differ from the slope of the correlation length by a factor of 2 which is in very good agreement (1.78 vs. 3.59).

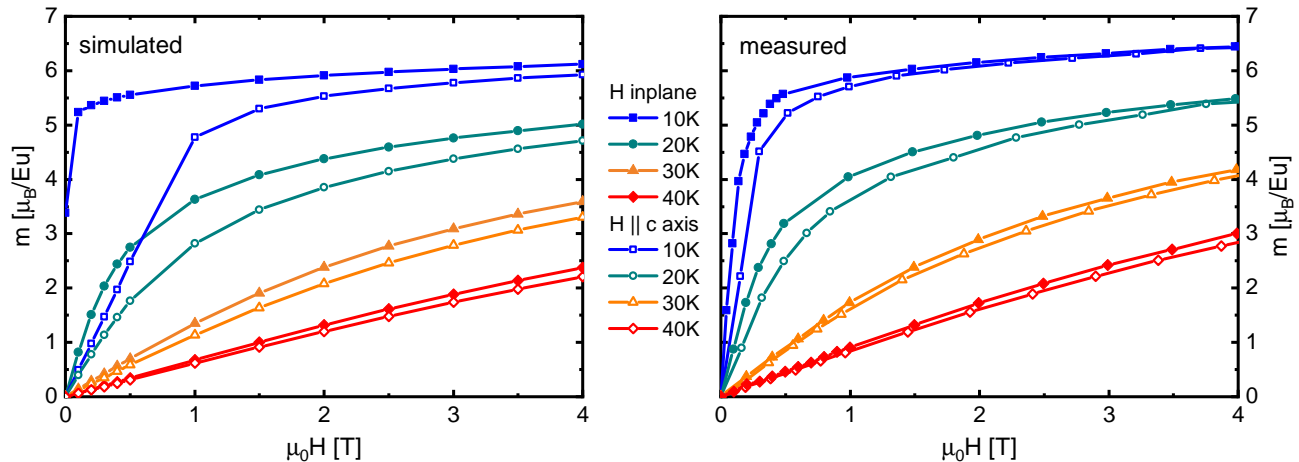


FIG. 7. Simulated (left) and measured (right) isothermal magnetization curves at $T = 10, 20, 30,$ and 40K , for fields applied in and out of the basal plane. The magnetization is normalized to the magnetization per Eu atom. The measured magnetization data as reprinted from Ref. [23] at temperatures below the superconducting transition were calculated from measured magnetization hysteresis curves by evaluating the symmetric part which in a first approximation removes the effects due to vortex pinning as described there.

Figure 7 presents the simulated and measured isothermal magnetization curves. The experimental magnetization data at temperatures below the superconducting transition were calculated from magnetization hysteresis curves by evaluating the symmetric part which in a first approximation removes the effects due to vortex pinning, as described in Ref. [23]. The isothermal magnetization shows an increasing anisotropy upon decreasing the temperature. Furthermore, the saturation field, i.e. the field where the magnetization reaches (almost) full polarization rapidly decreases with decreasing temperature. Below the magnetic transition, the simulation’s in-plane magnetization is non-zero even at zero magnetic field. This is an artifact of the system’s finite size; For its average to vanish—as expected for a BKT phase—an exponentially large simulation time is required. Overall, we find a very good agreement between the simulated and measured magnetization.

4. The role of magnetic anisotropy: From Heisenberg to 2D XY model

When tuning the parameter K from zero to large values, one can investigate the specific heat following different anisotropy strengths. For the isotropic case, $K = 0$, the specific heat features a hump, which is not associated with a phase transition. For a very large anisotropy $K \gg J$, the system’s response is equivalent to that of a 2D XY model, where the spin undergoes a BKT transition²⁹ at $k_B T/J = 1.04$. The specific heat curve reported by Gupta and co-workers in Ref. [29] is shown in Fig. 8 together with our simulation data. Note that we have accounted for a constant shift of $k_B/2$ (per spin) between the *true* XY model and a very anisotropic Heisenberg model, as spin waves normal to the spin plane (always existing for Heisenberg models but absent in the XY model) contribute a constant to the specific heat.

D: Anisotropy of Eu^{2+} moments due to exchange interaction with Fe electrons

The conventional mechanism of the crystalline anisotropy due to the spin-orbital LS interaction⁴⁷ is absent for Eu^{2+} ions, because these ions do not have an orbital moment L and their magnetic moment has purely spin origin. We identify the interaction of the Eu^{2+} moments with the Fe electrons as a possible source of crystalline anisotropy as modeled in Eq. (1). To illustrate this, we assume the exchange interaction between the Eu^{2+} spins S_i^{Eu} and spins

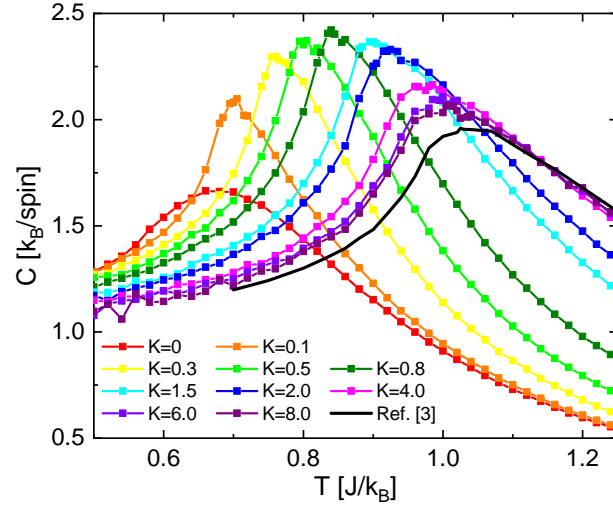


FIG. 8. specific heat (in units of k_B per spin) as a function of temperature ($k_B T/J$) for different crystal-anisotropies K (here in units of J). The black curve shows the result for the 2D XY model published in Ref. [29], shifted by 1/2 because of the additional harmonic degree of freedom (compared to a true XY system). The spin waves contribute $k_B/2$ per degree of freedom to the specific heat.

of electrons located on Fe d -orbitals, \mathbf{S}_j^{Fe} ,

$$\mathcal{H}_{\text{Eu-Fe}} = - \sum_{\langle i,j \rangle} \tilde{J}_{ij} \mathbf{S}_i^{\text{Eu}} \mathbf{S}_j^{\text{Fe}} \quad (\text{D1})$$

with \tilde{J}_{ij} being the Eu-Fe exchange constants. Assuming that the mechanism behind this Eu-Fe interaction is superexchange via As atoms, we observe that every Fe d -electron interacts with 12 Eu^{2+} spins (6 per layer) while every Eu^{2+} spin interacts with 24 Fe sites (12 per layer), see Fig. 9. In the related compounds without magnetic rare-earth layers, the response of the iron-arsenide layers to an external field \mathbf{H} is known to be anisotropic, see Refs. [32] (BaFe_2As_2) and [33] ($\text{CaKFe}_4\text{As}_4$), meaning that the local energy change of the iron subsystem caused by the magnetic field \mathbf{H} is $-\chi_x(H_x^2 + H_y^2) - \chi_z H_z^2/2$, where χ_x and χ_z are the magnetic susceptibilities per iron site. We should point out here that there are two possible contributions to the anisotropy of the magnetic susceptibility. The magnetic moment components of the iron d -electrons are related to their spin components as $m_\alpha^{\text{Fe}} = g_\alpha \mu_B S_\alpha^{\text{Fe}}$, while the response of S_α^{Fe} to the effective magnetic field $h_\alpha = g_\alpha \mu_B H_\alpha$ is determined by spin susceptibility $S_\alpha^{\text{Fe}} = \chi_\alpha^{\text{spin}} h_\alpha$. Both the g -factor and the spin susceptibility may be anisotropic due to spin-orbit interactions and they both contribute to the anisotropy of the magnetic susceptibility $\chi_\alpha = (g_\alpha \mu_B)^2 \chi_\alpha^{\text{spin}}$. As follows from Eq. (D1), the Eu^{2+} spins induce the effective field $\mathbf{h}_{\text{Eu},j} \equiv \sum_i \tilde{J}_{ij} \mathbf{S}_i^{\text{Eu}}$ on the iron subsystem yielding anisotropic nonlocal interaction of the form

$$\mathcal{H}_{\text{Fe}} = -\frac{1}{2} \sum_{\alpha,j} \chi_\alpha^{\text{spin}} \left(\sum_i \tilde{J}_{ij} S_{\alpha,i}^{\text{Eu}} \right) = -\frac{1}{2} \sum_{\alpha,j,i,k} \chi_\alpha^{\text{spin}} \tilde{J}_{ij} \tilde{J}_{kj} S_{\alpha,i}^{\text{Eu}} S_{\alpha,k}^{\text{Eu}}, \quad (\text{D2})$$

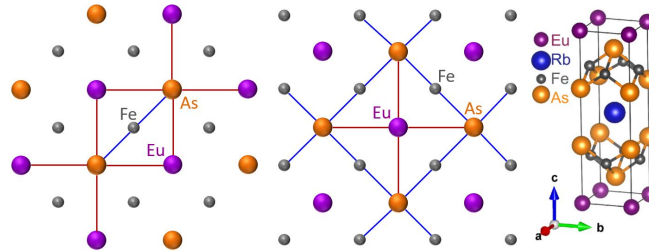


FIG. 9. Illustration of the superexchange interaction between Eu^{2+} spins and Fe d -electrons via As sites. Every Fe d -electron interacts with 6 Eu^{2+} spins per layer and every Eu^{2+} spin interacts with 12 Fe sites per layer.

which extends over several neighboring Eu sites. We also neglect here a possible nonlocality of iron-layer response. In the regime when the correlation length of Eu^{2+} moments exceeds the nonlocality range, we can approximate this interaction by a local one. In this case an anisotropy in the Eu subsystem is captured by the second term on the right-hand-side of Eq. (1) and we find an expression

$$K = \frac{\tilde{J}_{\text{eff}}^2}{4} (\chi_x^{\text{spin}} - \chi_z^{\text{spin}}) = \frac{\tilde{J}_{\text{eff}}^2}{4\mu_B^2} \left(\frac{\chi_x}{g_x^2} - \frac{\chi_z}{g_z^2} \right) \quad (\text{D3})$$

with the phenomenological constant with $\tilde{J}_{\text{eff}}^2 = \sum_{j,k} \tilde{J}_{ij} \tilde{J}_{kj} (S^{\text{Eu}})^2$. If we denote the nearest-neighbor and next-neighbor exchange constants by \tilde{J}_1 and \tilde{J}_2 respectively then $\tilde{J}_{\text{eff}}^2 = 32(\tilde{J}_1 + 2\tilde{J}_2)^2 (S^{\text{Eu}})^2$.

It would be interesting to evaluate the Eu-Fe exchange constant \tilde{J}_{eff} from Eq. (D3) and to compare it with the Eu-Eu exchange constant J . The reported susceptibilities for the iron moments in parent compounds, see Ref. [32] and [33] do not follow a Curie-Weiss law as expected for localized moments. Instead, for BaFe_2As_2 ³² the susceptibilities linearly increase with increasing temperature over a wide range (150-400K). Furthermore the difference between the two susceptibilities (along and perpendicular to c) is almost temperature-independent and amounts approximately to $\chi_x - \chi_z \approx 0.35 \times 10^{-3} \text{emu/G mol}$. In the compound $\text{CaKFe}_4\text{As}_4$, which has the same structure as $\text{RbEuFe}_4\text{As}_4$, the susceptibilities behave somewhat differently³³. In this case the susceptibilities linearly decrease with increasing temperature and their relative difference shrinks for higher temperature. Near the superconducting transition $\chi_x - \chi_z \approx 10^{-3} \text{emu/G mol}$. Unfortunately, this information is not sufficient for an unambiguous evaluation of the Eu-Fe exchange constant from Eq. (D3) because the g -factors of the Fe d -electrons remain unknown. If we make the simplest assumptions $g_x = g_z = 2$ and $\tilde{J}_2 \approx \tilde{J}_1/2$, we obtain $\tilde{J}_1 \sim 0.3J$, i.e. the Eu-Fe and Eu-Eu exchange strengths are comparable.

- ¹ K.-H. Muller and V. N. Narozhnyi, *Interaction of superconductivity and magnetism in borocarbide superconductors*, Reports on Progress in Physics **64**, 943 (2001).
- ² M. L. Kulić and A. I. Buzdin, *Coexistence of singlet superconductivity and magnetic order in bulk magnetic superconductors and sf heterostructures*, in *Superconductivity: Conventional and Unconventional Superconductors*, edited by K. H. Bennemann and J. B. Ketterson (Springer Berlin Heidelberg, Berlin, Heidelberg, 2008) p. 163.
- ³ S. Zapf and M. Dressel, *Europium-based iron pnictides: a unique laboratory for magnetism, superconductivity and structural effects*, Reports on Progress in Physics **80**, 016501 (2017).
- ⁴ G. Cao, S. Xu, Z. Ren, S. Jiang, C. Feng, and Z. Xu, *Superconductivity and ferromagnetism in $\text{EuFe}_2(\text{As}_{1-x}\text{P}_x)_2$* , Journal of Physics: Condensed Matter **23**, 464204 (2011); H. S. Jeevan, D. Kasinathan, H. Rosner, and P. Gegenwart, *Interplay of antiferromagnetism, ferromagnetism, and superconductivity in $\text{EuFe}_2(\text{As}_{1-x}\text{P}_x)_2$ single crystals*, Physical Review B **83**, 054511 (2011).
- ⁵ H. S. Jeevan, Z. Hossain, D. Kasinathan, H. Rosner, C. Geibel, and P. Gegenwart, *High-temperature superconductivity in $\text{Eu}_{0.5}\text{K}_{0.5}\text{Fe}_2\text{As}_2$* , Physical Review B **78**, 092406 (2008).
- ⁶ Y. Qi, Z. Gao, L. Wang, D. Wang, X. Zhang, and Y. Ma, *Superconductivity at 34.7K in the iron arsenide $\text{Eu}_{0.7}\text{Na}_{0.3}\text{Fe}_2\text{As}_2$* , New Journal of Physics **10**, 123003 (2008).
- ⁷ Y. Liu, Y.-B. Liu, Q. Chen, Z.-T. Tang, W.-H. Jiao, Q. Tao, Z.-A. Xu, and G.-H. Cao, *A new ferromagnetic superconductor: $\text{CsEuFe}_4\text{As}_4$* , Science Bulletin **61**, 1213 (2016).
- ⁸ Y. Liu, Y.-B. Liu, Z.-T. Tang, H. Jiang, Z.-C. Wang, A. Ablimit, W.-H. Jiao, Q. Tao, C.-M. Feng, Z.-A. Xu, and G.-H. Cao, *Superconductivity and ferromagnetism in hole-doped $\text{RbEuFe}_4\text{As}_4$* , Phys. Rev. B **93**, 214503 (2016).
- ⁹ V. L. Berezinskii, *Destruction of long-range order in one-dimensional and two-dimensional systems having a continuous symmetry group. I. Classical systems*, [Zh. Eksp. Teor. Fiz. **59**, 907 (1971)] JETP **32**, 493 (1971).
- ¹⁰ J. M. Kosterlitz and D. J. Thouless, *Ordering, metastability and phase transitions in two-dimensional systems*, Journal of Physics C: Solid State Physics **6**, 1181 (1973).
- ¹¹ J. M. Kosterlitz, *The critical properties of the two-dimensional xy model*, Journal of Physics C: Solid State Physics **7**, 1046 (1974).
- ¹² K. Hirakawa, H. Yoshizawa, and K. Ubukoshi, *Neutron Scattering Study of the Phase Transition in Two-Dimensional Planar Ferromagnet K_2CuF_4* , J. Phys. Soc. Jpn. **51**, 2151 (1982).
- ¹³ K. Hirakawa, *Kosterlitz-Thouless transition in two-dimensional planar ferromagnet K_2CuF_4 (invited)*, J. Appl. Phys. **53**, 1893 (1982).
- ¹⁴ C. A. Cornelius, P. Day, P. J. Fyne, M. T. Hutchings, and P. J. Walker, *Temperature and field dependence of the magnetisation of Rb_2CrCl_4 : a two-dimensional easy-plane ionic ferromagnet*, J. Phys. C: Solid State Phys. **19**, 909 (1986).
- ¹⁵ S. Bramwell, P. Holdsworth, and M. Hutchings, *Static and Dynamic Magnetic Properties of Rb_2CrCl_4 : Ideal 2D-XY Behaviour in a Layered Magnet*, J. Phys. Soc. Jpn. **64**, 3066 (1995).
- ¹⁶ H. S. Jeevan, Z. Hossain, D. Kasinathan, H. Rosner, C. Geibel, and P. Gegenwart, *Electrical resistivity and specific heat of single-crystalline EuFe_2As_2 : A magnetic homologue of SrFe_2As_2* , Phys. Rev. B **78**, 052502 (2008).
- ¹⁷ Z. Ren, Z. Zhu, S. Jiang, X. Xu, Q. Tao, C. Wang, C. Feng, G. Cao, and Z. Xu, *Antiferromagnetic transition in EuFe_2As_2 : A possible parent compound for superconductors*, Phys. Rev. B **78**, 052501 (2008).
- ¹⁸ U. B. Paramanik, P. L. Paulose, S. Ramakrishnan, A. K. Nigam, C. Geibel, and Z. Hossain, *Magnetic and superconducting properties of Ir-doped EuFe_2As_2* , Superconductor Science and Technology **27**, 075012 (2014).
- ¹⁹ A. Oleaga, A. Salazar, A. Thamizhavel, and S. Dhar, *Thermal properties and ising critical behavior in EuFe_2As_2* , Journal of Alloys and Compounds **617**, 534 (2014).
- ²⁰ J. Wosnitzer, *From thermodynamically driven phase transitions to quantum critical phenomena*, Journal of Low Temperature Physics **147**, 249 (2007).
- ²¹ M. Bouvier, P. Lethuillier, and D. Schmitt, *Specific heat in some gadolinium compounds. i. experimental*, Phys. Rev. B **43**, 13137 (1991).
- ²² D. C. Johnston, R. J. McQueeney, B. Lake, A. Honecker, M. E. Zhitomirsky, R. Nath, Y. Furukawa, V. P. Antropov, and Y. Singh, *Magnetic exchange interactions in BaMn_2As_2 : A case study of the J_1 - J_2 - J_c Heisenberg model*, Phys. Rev. B **84**, 094445 (2011).
- ²³ M. P. Smylie, K. Willa, J.-K. Bao, K. Ryan, Z. Islam, H. Claus, Y. Simsek, Z. Diao, A. Rydh, A. E. Koshelev, W.-K. Kwok, D. Y. Chung, M. G. Kanatzidis, and U. Welp, *Anisotropic superconductivity and magnetism in single-crystal $\text{RbEuFe}_4\text{As}_4$* , Phys. Rev. B **98**, 104503 (2018).
- ²⁴ V. S. Stolyarov, A. Casano, M. A. Belyanchikov, A. S. Astrakhantseva, S. Y. Grebenchuk, D. S. Baranov, I. A. Golovchanskiy, I. Voloshenko, E. S. Zhukova, B. P. Gorshunov, A. V. Muratov, V. V. Dremov, L. Y. Vinnikov, D. Roditchev, Y. Liu, G.-H. Cao, M. Dressel, and E. Uykur, *Unique interplay between superconducting and ferromagnetic orders in $\text{EuRbFe}_4\text{As}_4$* , Phys. Rev. B **98**, 140506 (2018).
- ²⁵ N. Metropolis, A. W. Rosenbluth, M. N. Rosenbluth, A. H. Teller, and E. Teller, *Equation of state calculations by fast computing machines*, The Journal of Chemical Physics **21**, 1087 (1953).
- ²⁶ W. K. Hastings, *Monte Carlo sampling methods using Markov chains and their applications*, Biometrika **57**, 97 (1970).
- ²⁷ J. Tobochnik and G. V. Chester, *Monte carlo study of the planar spin model*, Phys. Rev. B **20**, 3761 (1979).
- ²⁸ W. Janke and T. Matsui, *Crossover in the XY model from three to two dimensions*, Phys. Rev. B **42**, 10673 (1990).
- ²⁹ R. Gupta and C. F. Baillie, *Critical behavior of the two-dimensional xy model*, Physical Review B **45**, 2883 (1992).
- ³⁰ A. Cuccoli, V. Tognetti, P. Verrucchi, and R. Vaia, Phys. Rev. B **51**, 12840 (1995).
- ³¹ P. Sengupta, A. W. Sandvik, and R. R. P. Singh, *Specific heat of quasi-two-dimensional antiferromagnetic heisenberg models with varying interplanar couplings*, Phys. Rev. B **68**, 094423 (2003).

- ³² X. F. Wang, T. Wu, G. Wu, H. Chen, Y. L. Xie, J. J. Ying, Y. J. Yan, R. H. Liu, and X. H. Chen, *Anisotropy in the Electrical Resistivity and Susceptibility of Superconducting BaFe₂As₂ Single Crystals*, Physical Review Letters **102**, 117005 (2009).
- ³³ W. R. Meier, T. Kong, U. S. Kaluarachchi, V. Taufour, N. H. Jo, G. Drachuck, A. E. Böhmer, S. M. Saunders, A. Sapkota, A. Kreyssig, M. A. Tanatar, R. Prozorov, A. I. Goldman, F. F. Balakirev, A. Gurevich, S. L. Bud'ko, and P. C. Canfield, *Anisotropic thermodynamic and transport properties of single-crystalline CaKFe₄As₄*, Phys. Rev. B **94**, 064501 (2016).
- ³⁴ Y. Xiao, Y. Su, W. Schmidt, K. Schmalzl, C. M. N. Kumar, S. Price, T. Chatterji, R. Mittal, L. J. Chang, S. Nandi, N. Kumar, S. K. Dhar, A. Thamizhavel, and T. Brueckel, *Field-induced spin reorientation and giant spin-lattice coupling in EuFe₂As₂*, Phys. Rev. B **81**, 220406 (2010).
- ³⁵ S. Hikami and T. Tsuneto, *Phase transition of quasi-two dimensional planar system*, Progr. Theor. Phys. **63**, 387 (1980).
- ³⁶ A. Polyakov, *Interaction of goldstone particles in two dimensions. Applications to ferromagnets and massive Yang-Mills fields*, Physics Letters B **59**, 79 (1975).
- ³⁷ E. Brézin and J. Zinn-Justin, *Renormalization of the nonlinear σ model in $2 + \epsilon$ dimensions—application to the heisenberg ferromagnets*, Physical Review Letters **36**, 691 (1976); *Spontaneous breakdown of continuous symmetries near two dimensions*, Physical Review B **14**, 3110 (1976).
- ³⁸ D. R. Nelson and R. A. Pelcovits, *Momentum-shell recursion relations, anisotropic spins, and liquid crystals in $2 + \epsilon$ dimensions*, Physical Review B **16**, 2191 (1977).
- ³⁹ S. H. Shenker and J. Tobochnik, *Monte Carlo renormalization-group analysis of the classical Heisenberg model in two dimensions*, Physical Review B **22**, 4462 (1980).
- ⁴⁰ T. Nagamiya, K. Nagata, and Y. Kitano, *Magnetization Process of a Screw Spin System*, Progress of Theoretical Physics **27**, 1253 (1962).
- ⁴¹ D. C. Johnston, *Magnetic structure and magnetization of helical antiferromagnets in high magnetic fields perpendicular to the helix axis at zero temperature*, Physical Review B **96**, 104405 (2017).
- ⁴² V. Vlasko-Vlasov, A. E. Koshelev, M. P. Smylie, J.-K. Bao, D. Y. Chung, M. G. Kanatzidis, U. Welp, and W.-K. Kwok, *Self-induced Magnetic Flux Structure in the Magnetic Superconductor RbEuFe₄As₄*, arXiv:1902.08125 (2019).
- ⁴³ M. B. Maple, H. C. Hamaker, L. D. Woolf, H. B. Mackay, Z. Fisk, W. Odoni, and H. R. Ott, *Crystalline Electric Field and Structural Effects in f-Electrons Systems*, edited by J. E. Crow, R. P. Guertin, and T. W. Mihalisin (New York: Plenum Press, 1980) pp. 533–543.
- ⁴⁴ J.-K. Bao, K. Willa, M. P. Smylie, H. Chen, U. Welp, D. Y. Chung, and M. G. Kanatzidis, *Single crystal growth and study of the ferromagnetic superconductor RbEuFe₄As₄*, Crystal Growth & Design **18**, 3517 (2018).
- ⁴⁵ S. Tagliati, V. M. Krasnov, and A. Rydh, *Differential membrane-based nanocalorimeter for high-resolution measurements of low-temperature specific heat*, Rev. Sci. Instrum. **83**, 055107 (2012).
- ⁴⁶ K. Willa, Z. Diao, D. Campanini, U. Welp, R. Divan, M. Hudl, Z. Islam, W.-K. Kwok, and A. Rydh, *Nanocalorimeter platform for in situ specific heat measurements and x-ray diffraction at low temperature*, Review of Scientific Instruments **88**, 125108 (2017).
- ⁴⁷ R. M. White, *Quantum Theory of Magnetism* (Spinger, 2007).